



Validation of a Transcriptome-Based Assay for Classifying Cancers of Unknown Primary Origin

Jackson Michuda¹ · Alessandra Breschi¹ · Joshua Kapilivsky¹ · Kabir Manghnani¹ · Calvin McCarter¹ · Adam J. Hockenberry¹ · Brittany Mineo¹ · Catherine Igartua¹ · Joel T. Dudley¹ · Martin C. Stumpe¹ · Nike Beaubier¹ · Maryam Shirazi¹ · Ryan Jones¹ · Elizabeth Morency¹ · Kim Blackwell¹ · Justin Guinney¹ · Kyle A. Beauchamp¹ · Timothy Taxter¹

Accepted: 2 April 2023 / Published online: 26 April 2023
© The Author(s) 2023

Abstract

Introduction Cancers assume a variety of distinct histologies, and may originate from a myriad of sites including solid organs, hematopoietic cells, and connective tissue. Clinical decision-making based on consensus guidelines such as the National Comprehensive Cancer Network (NCCN) is often predicated on a specific histologic and anatomic diagnosis, supported by clinical features and pathologist interpretation of morphology and immunohistochemical (IHC) staining patterns. However, in patients with nonspecific morphologic and IHC findings—in addition to ambiguous clinical presentations such as recurrence versus new primary—a definitive diagnosis may not be possible, resulting in the patient being categorized as having a cancer of unknown primary (CUP). Therapeutic options and clinical outcomes are poor for patients with CUP, with a median survival of 8–11 months.

Methods Here, we describe and validate the Tempus Tumor Origin (Tempus TO) assay, an RNA-sequencing-based machine learning classifier capable of discriminating between 68 clinically relevant cancer subtypes. Model accuracy was assessed using primary and/or metastatic samples with known subtype.

Results We show that the Tempus TO model is 91% accurate when assessed on both a retrospectively held out cohort and a set of samples sequenced after model freeze that collectively contained 9210 total samples with known diagnoses. When evaluated on a cohort of CUPs, the model recapitulated established associations between genomic alterations and cancer subtype.

Discussion Combining diagnostic prediction tests (e.g., Tempus TO) with sequencing-based variant reporting (e.g., Tempus xT) may expand therapeutic options for patients with cancers of unknown primary or uncertain histology.

1 Introduction

Accurate characterization of primary tissue origin, histology, and clinical/pathologic stage is required for assigning effective therapeutic interventions for patients with cancer [1]. However, some patients present with ambiguous clinical and histologic findings and no definitive primary site of disease [2]. These tumors are a heterogeneous group known as cancers of unknown primary (CUP) and account for 2–5% of cancers [3, 4]. The American Cancer Society estimates

Key Points

Using RNA expression data from > 50,000 tumor biopsies, we developed and validated a predictive model, for use in the setting of cancers of unknown primary, that is capable of discriminating between 68 possible histological subtypes.

Our model is highly accurate on both retrospective (data that were withheld from training, 91.2% accuracy) and a labeled dataset that was sequenced after model training was completed (91.0% accuracy), and this accuracy is robust against imputed metastatic status and tumor purity.

Our model is also extensible, showing high accuracy (84.3%) on a fully independent dataset (TCGA).

✉ Kyle A. Beauchamp
kyle.beauchamp@tempus.com

✉ Timothy Taxter
tim@tempus.com

Extended author information available on the last page of the article

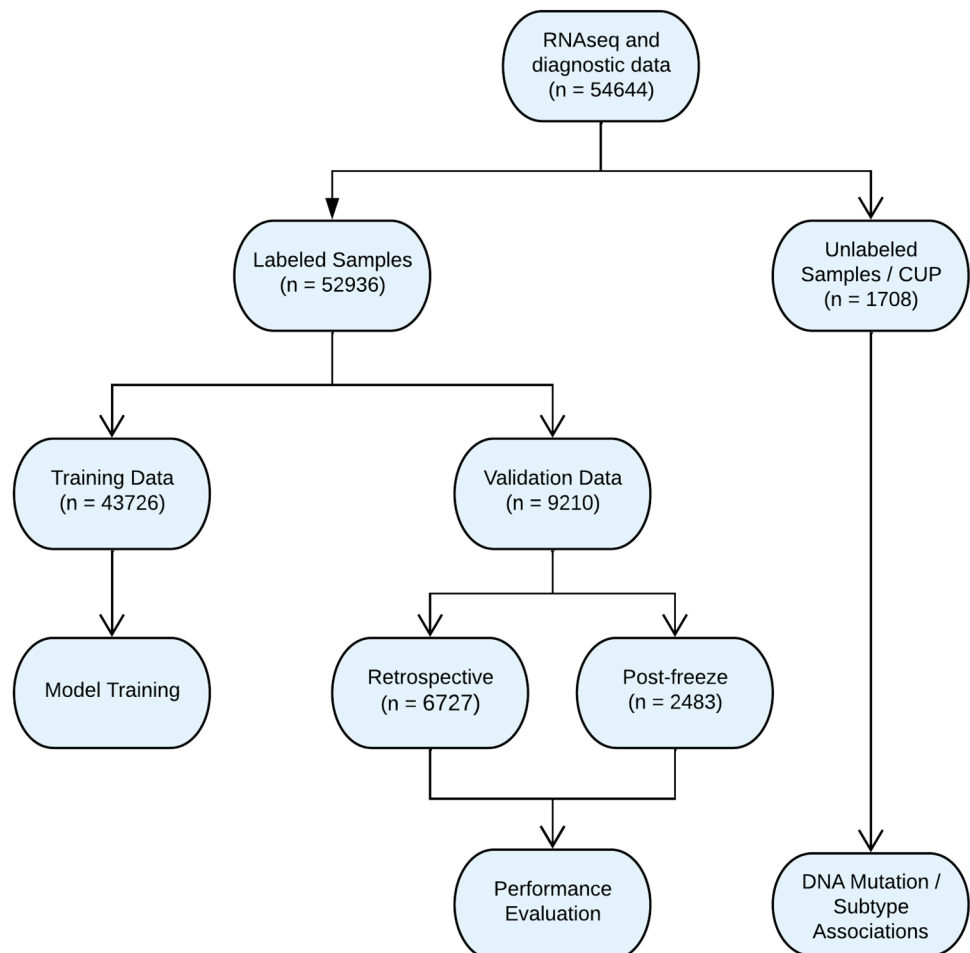
that over 30,000 patients will be diagnosed with CUP in 2021 [5, 6]. For patients with CUP, the average survival time is typically 8–12 months after diagnosis, though some subgroups may survive for up to 12–36 months [4]. Establishing why certain patients with CUP have more favorable prognoses and improving survival for all patients with CUP is a key goal for clinicians [7, 8].

Although direct examination of tissue—via morphology and immunohistochemistry—has long guided cancer type diagnosis, advances in sequencing technologies have facilitated new ways of characterizing cancer [9, 10]. These approaches have further enabled the development of several molecular diagnostics aimed at determining tumor origin specifically [11]. Methods for tumor classification may rely on microRNA signatures [12, 13], transcript expression [14–16], mutation profiling via DNA sequencing [17, 18], methylation profiling [19], or whole-slide histology imaging [20]. For example, one commercially available assay leverages RT–PCR of 92 genes and a machine learning algorithm to differentiate between 50 tumor subtypes [21–24]. Another assay developed a 2000 gene microarray-based RNA classifier

and demonstrated 89% accuracy in predicting 15 tissue types [14]. More recently, one machine learning classifier using whole-transcriptome RNA sequencing demonstrated an accuracy of 86% in predicting 66 cancer/tissue types [15], while another demonstrated high test set (97%) and external accuracy (72–87%) [16]. Common to all these approaches is the ability to accurately predict cancer subtypes; however, direct comparisons of these studies are challenged by differing numbers of predicted subtypes and variation in generalization performance.

While prior studies and assays have made important advances, there are key limitations [11]. For instance, DNA-based panels [17] perform well when a tumor has a canonical alteration associated with a specific cancer type or subtype, but fail in their absence. RT–PCR assays that profile a subset of the transcriptome have limited accuracy when a tumor does not express a lineage-specific gene [23, 24]. Other assays can predict tissue of origin, but lack finer granularity such as site-specific subtype or histology; this lack of specificity may be inadequate for some treatment or diagnostic decisions. Multi-omic machine learning architectures that integrate data from multiple assays may

Fig. 1. CONSORT diagram describing the cohorts used for classifier training, accuracy evaluation on labeled samples (validation data, including both retrospective and post-freeze samples), and assessment on unlabeled CUP samples



provide an opportunity for accuracy improvement and can help alleviate concerns with using single data types [25], but these models require complex algorithms for data integration. Finally, even IHC—the current standard of care in making CUP diagnoses—is limited by the frequent loss of cell markers during de-differentiation and oncogenesis [26].

By contrast, full-transcriptome RNA sequencing (RNA-seq) overcomes several of these limitations. As shown in prior work using methylation [19] and gene expression [23, 24] models, cancer cells retain an epigenetic and transcriptional signature of their cell type of origin. Next-generation sequencing (NGS) has facilitated the adoption of transcriptome-wide expression profiling in a clinical setting owing to relatively low costs and minimal sample preparation. Hybrid capture assays, with probes covering the whole exome, can accurately extract expression profiles from small formalin-fixed paraffin-embedded (FFPE) tissue biopsies. Expression data generated by transcriptome-wide RNA-seq are well suited for machine learning and statistical modeling due to their quantitative, high dimensional, and untargeted nature [27].

Here, we describe and validate an RNA expression-based tumor diagnosis classifier trained on whole-exome capture RNA-seq data from 43,726 tumor samples. This machine learning model distinguishes 68 tumor subtypes—a more comprehensive and finer level of subtype resolution than previous studies [17, 23, 25]. These tumor subtypes include neuroendocrine subtypes, sarcoma subtypes, and site-specific histologies to allow for precise application of medical guidelines. The classifier is highly accurate (91%) on an independent validation dataset, and is robust to primary versus metastatic lesions and tumor purity.

2 Materials and Methods

2.1 Cohort

Cohort selection for training and validation is summarized in Fig. 1. The principal inclusion criterion was the availability of quality-controlled RNA-sequencing of a tumor specimen—no normal tissue samples were included in the development, validation, or use-case of the model. A summary of assay quality controls is described in the “RNA-seq assay” section. No restrictions on the cancer stage or site of biopsy were applied. Biospecimen material was restricted to FFPE, bone marrow, and blood. Allowed cancer types and subtypes are described in the section “Diagnostic subtype assignment.” Samples were either labeled with known subtype (cancers of known primary) ($N=52,936$, comprising 68 subtypes) or marked as unlabeled (e.g., CUP) ($N=1,708$). Labeled samples were split into 75%/25% training and validation cohorts via stratified random sampling (matching subtype

distributions), which were used for model training and evaluation, respectively. The validation cohort was an independent test set of tumors derived from different patients and samples than the training data. A comparison of the tissue and subtype distributions in the training and validation sets is provided in Supplementary Tables S1 and S2. In the event that a patient had multiple biopsies, they were all grouped into either the training or validation cohorts to prevent information leakage. The validation cohort consisted of both retrospective samples that were sequenced prior to the model training date, as well as a set of samples sequenced after model development and training. The unlabeled (CUP) cohort consisting of diagnostically ambiguous tumors was not used in the primary performance analysis, but was analyzed as part of the mutation-subtype enrichment study.

2.2 RNA-Seq Assay

As part of the Tempus xT next-generation sequencing assay, CAP/CLIA validated hybrid capture RNA-seq was used to generate transcriptome-wide expression data from paraffinized tissue [28, 29]. A hybrid capture-based protocol was utilized instead of traditional poly-A capture to overcome the RNA fragmentation associated with tissue formalin fixation and paraffinization [30]. Briefly, FFPE samples (typically blocks) were cut into slides 4 μm thick and reviewed by a pathologist. Samples of adequate quality—with a minimum tumor fraction of 20% after microdissection when required—underwent RNA extraction. Extraction quality was assessed using a fragment analyzer and quantity was assessed using a fluorescent nucleic acid stain and a fluorescence microplate reader. At least 50 ng of RNA was extracted before proceeding to library preparation. Library preparation included steps for complementary strand synthesis with reverse transcriptase, ligation of dual indexed unique molecular identifier (UMI) adapters, and PCR amplification. At least 150 ng of amplified cDNA was required to proceed to hybridization. cDNA fragments were captured using a full exome panel [31] and sequenced on a NovaSeq 6000 (Illumina Inc, San Diego, CA) to a minimum depth of 30 million reads.

Following sequencing, raw BCL files were used to generate FASTQ files using BCL2FASTQ (v2.17). Adapters were trimmed using Skewer (v0.2.2). Reads were then aligned with STAR (v.2.5.4a) to generate BAM files and undergo UMI deduplication with umitools (v1.0.1). Following deduplication, samples were converted to FASTQ files using bedtools (v2.27.1) before undergoing quantification using Kallisto (v0.44.0) with the Ensembl GRCH37 reference transcriptome [28, 29].

2.3 Feature Engineering

Raw RNA expression data were normalized to minimize the effect of technical artifacts such as GC content, transcript length, and library size [28, 29]. This normalization strategy is similar to the one employed in DESeq [32], with the important distinction being that our approach allows us to train the normalization on our training dataset and apply it to a fully held validation dataset, as required for machine learning research. In addition, a batch correction method was used to account for small technical differences between two versions of the RNA-seq assay, including a modified exome capture probe set and the addition of UMIs. The batch correction method leverages more than 500 paired samples that were run on both assays to match the means and variances of normalized expression (for details, see Supplementary Methods). In this work, all validation statistics refer to the most recent assay version.

The 20,061-dimensional gene-level expression features underwent several threshold-based filters and data scalings. Low variance genes were removed using a threshold of 0.176; 6014 features remained after filtering. Genes with low interassay correlation were removed using a threshold of 0.725; 17,513 features remained after applying this filter. Finally, expression data were scaled to have a uniform mean and variance per gene. The optimal thresholds for establishing low variance and interassay reproducibility filtering were tuned via a hyperparameter grid search, as described in detail below. In all, the application of both filters led to 5498 genes in the final feature set. To prevent information leakage, all transformation parameters were learned using the training set and independently applied to the validation set.

2.4 Expression Validation

Gene expression features were analytically validated [33] to ensure that the model relied on accurate and reproducible inputs. Universal Human Reference (UHR) RNA [34] was sequenced on the Tempus RNA-seq assay to establish linearity against an orthogonal method. Normalized gene expression values were compared against a reference set of 17,321 qPCR Δ CT values established by the MAQC consortium. Normalized expression data were generated for 21 UHR replicates. All replicates had a Pearson's correlation coefficient (R value) greater than 0.76 between the Δ CT values and gene expression data. Further methodological validation included a per-gene linearity study using 88 clinical samples and testing 18 genes to measure concordance between qPCR Δ CT values and normalized gene expression levels (Supplementary Fig. S1). The 18 genes were selected due to their high variance across different tumor types, relevance to cancer, and associations

with clinically relevant amplifications. Of these, 15/18 genes had an R value > 0.75 . All genes had an R value greater than 0.5, and the lowest performing genes were those with a small Δ CT dynamic range. In genes with large dynamic range, gene expression profiling with RNA-seq is highly concordant with qPCR.

2.5 Diagnostic Subtype Assignment

Samples were annotated with one of 68 subtypes (in this work, a subtype is defined as a site-specific histology) inclusive of cancer types and histologic subtypes. Samples were annotated with clinical and diagnostic information in two ways. Each sample underwent pathology review by a board-certified pathologist. The pathologist's workflow included reviewing a patient's clinical documents (such as progress notes and external pathology reports, which includes diagnostic IHC), viewing H&E-stained images, and inputting free-text diagnostic data describing the primary site, histological subtype, and biopsy site into the laboratory information management system for a sample. Patient records underwent a second round of clinical data review by trained abstractors to generate standardized diagnostic data for a patient. Abstractors reviewed a patient's clinical notes within a document review platform and assigned Unified Medical Language System codes to describe a patient's clinical history of diagnosis.

From an analysis of this corpus of real-world diagnostic data, a curated set of diagnoses was developed to achieve broad coverage over, and clinical differentiation of, clinically meaningful cancer subtypes and histologies. In total, 68 diagnostic labels (Supplementary Table S3) were developed. To assign diagnostic labels to each sample, a natural language model consisting of regular expressions was used to parse the free text diagnostic field assigned by the pathologist into a label. A rules-based system was designed to identify diagnostically ambiguous cases where a definitive subtype could not be confidently assigned. Diagnostically ambiguous samples (e.g., samples matching zero or several subtypes) were excluded from the labeled model training and validation sets, but were considered in the analysis of the CUP cohort.

A de-identified case review by pathologists was used to assess the accuracy of automated subtype assignments. Three different pathologists were presented with de-identified clinical data from 118 cases (1 case from each of the subtypes and 50 additional cases selected at random). Each pathologist reviewed the clinical data and was instructed to assign a single subtype to each case from the set of 68 labels.

2.6 Machine Learning Model

The machine learning model is a multinomial logistic regression classifier with L2 regularization. To overcome class imbalance in the training set, rare classes were upweighted. The weights for the i th class are given as $w_i = \frac{n_i^\alpha}{\sum_j n_j^\alpha}$, where n_i is the observed count of class i and α is a smoothing parameter that was determined via hyperparameter search. Including the previously mentioned feature engineering, the hyperparameter grid search was performed via three-fold cross-validation (evaluated using the log loss metric) on the training set that simultaneously assessed (1) L2 regularization strength, (2) variance threshold, (3) interassay concordance threshold, and (4) class weight smoothing parameter.

2.7 Validation Metrics

Models were evaluated using three metrics computed on the independent validation set: accuracy, top-three accuracy, and mean sensitivity. Accuracy and top-three accuracy were computed as the average (over samples) of the number of times the true subtype assignment was found in the top one or any of the top three highest probability subtype predictions, respectively. Mean sensitivity was computed by first calculating the sensitivity [TP/(TP+FN)] within each subtype, and then taking the unweighted mean across all 68 subtypes. Binomial confidence intervals for metrics were estimated using Markov chain Monte Carlo. Per-label specificity [TN/(TN + FP)] was also computed within each subtype.

2.8 TCGA Assessment

To assess the generalizability of our model beyond samples sequenced in our laboratory, we evaluated the performance of the TO classifier using data generated by The Cancer Genome Atlas (TCGA) [35].

First, tabular clinical data for all TCGA studies were downloaded from the GDC data portal (<https://portal.gdc.cancer.gov/>). Next, a crosswalk was constructed to map each unique TCGA subtype (i.e., each of the 617 unique combinations of TCGA study, ICD10 code, primary diagnosis, site of resection, and tissue of origin) to the appropriate Tempus TO subtype (Supplementary Table S4). Subtypes with conflicting diagnostic information or no Tempus equivalent were labeled “Other” and excluded from analysis. Overall, 33 TCGA studies were mapped to 38 Tempus TO subtypes (Supplementary Table S5). One notable example of the histology-by-histology mapping was TCGA type “sarc,” which was mapped onto five

distinct Tempus TO sarcoma subtypes. Another example is the TCGA typing for colon (“coad”) and rectal (“read”) carcinomas, which were mapped to Tempus TO subtype “colorectal adenocarcinoma”; this lumping is consistent with analysis of these TCGA types presented in the TCGA publication [36], which combined the types during analysis.

After obtaining the crosswalk, the diagnostic subtypes specified by TCGA were mapped to obtain a comparable set of internally defined subtype labels for each TCGA sample. The RNA-sequencing results from TCGA fastqs (9976 samples) were processed using Kallisto and normalized at the gene level with the same reference for consistency with other data used in this work. Finally, the subtype classifier was applied to each sample in TCGA to obtain a predicted subtype and performance was assessed using the same metrics described above.

2.9 DNA Sequencing Assay

Each sample also underwent co-isolation of nucleic acids to generate both DNA and RNA material for sequencing. DNA was sequenced using a targeted sequencing panel (Tempus xT) [29]. The assay has an average coverage of 500× and detects single nucleotide variants (SNVs), indels, and copy number variants in 595–648 genes spanning 3.6 Mb of genomic space. DNA data was not used as input into the gene expression-based model, so it provides an orthogonal method to aid in diagnostic interpretation and for evaluation of self-consistency on CUP samples.

2.10 Mutation Subtype Associations

Mutation subtype enrichments were used to characterize classifier behavior on CUP samples without a definitive clinical diagnosis. First, somatic mutations were aggregated for two cohorts: samples with a subtype diagnosis and samples without (CUP samples). For samples with a known subtype, Fisher’s exact test was used to find all subtype gene pairs with significant enrichments. A significant enrichment was defined as an association (i.e., an odds ratio calculated from the contingency table between subtype and mutation status) with a one-sided p -value less than 1.6×10^{-6} (i.e., an alpha

Table 1. Model performance metrics on a held-out set of labeled samples

	Validation
Sample size	9210
Accuracy	91.1%
Top three accuracy	97.5%
Mean sensitivity	80.0%

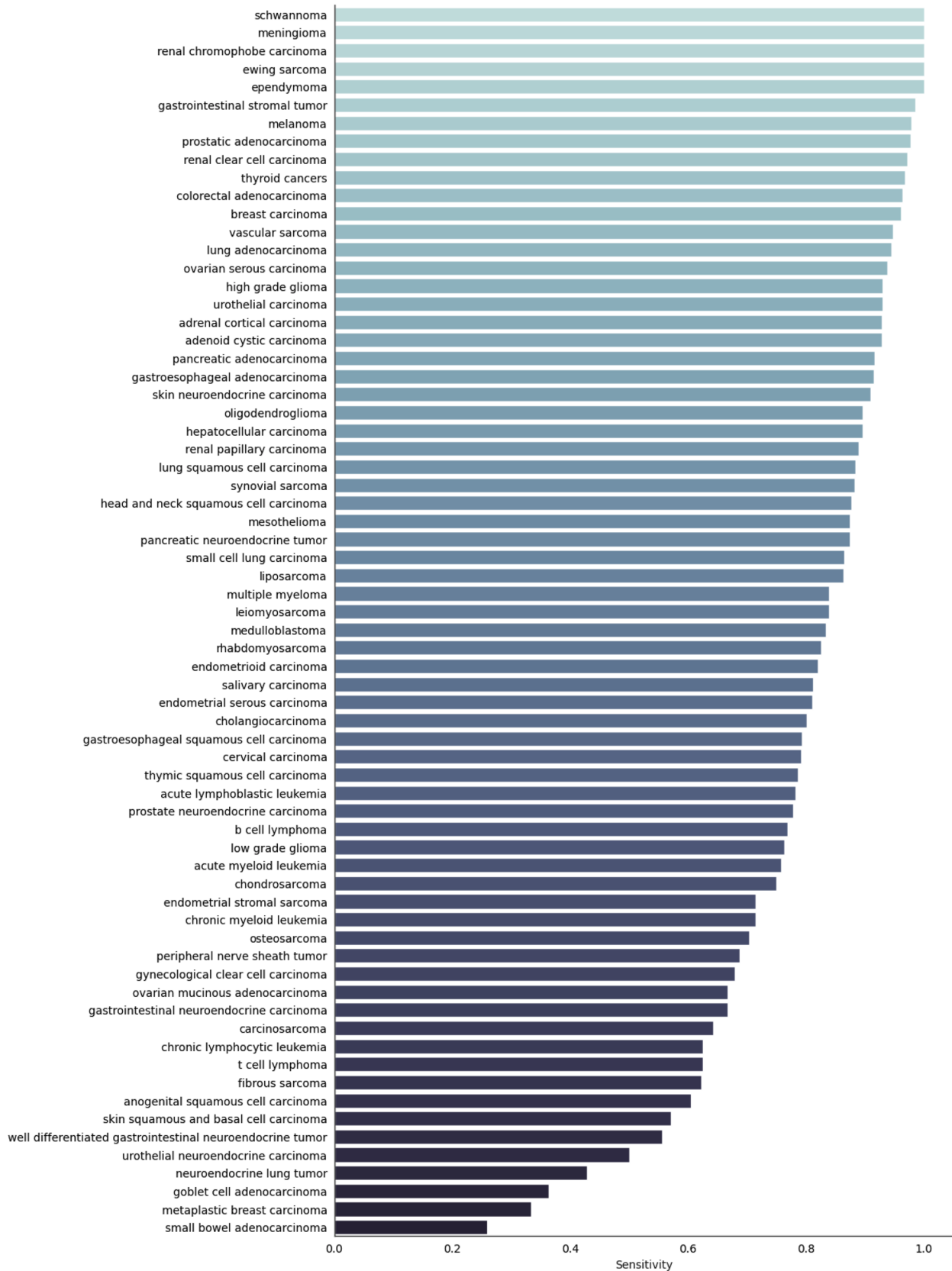


Fig. 2. Sensitivity for each of the 68 possible subtypes sorted from highest to lowest. See Supplementary Table S3 for full results

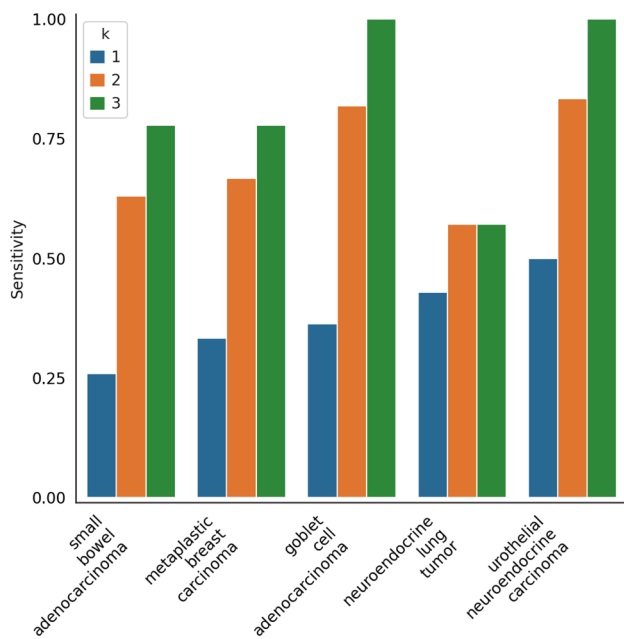


Fig. 3 The top- k sensitivity ($k = 1, 2, 3$) for the most difficult-to-predict subtypes highlights that the correct prediction is frequently in the top two or top three predictions

of 0.05 using the Bonferroni correction with 30,804 comparisons, obtained by considering 453 genes with observed mutations for one of the 68 labels). Significant enrichments were further filtered on the basis of their frequency; subtype–gene pairs with insufficient statistical power in the CUP cohort were removed by excluding pairs for which the probability of observing zero mutant counts (assuming identical mutant frequencies across labeled and CUP cohorts) was below 0.05. Finally, the list of significant associations (from known subtypes) was then evaluated on the classifier-predicted subtypes in the CUP cohort. Somatic mutation frequencies were estimated as the fraction of samples with a mutation in each gene.

3 Results

3.1 Label Accuracy

We compiled an initial dataset containing 54,644 tumor-derived RNA-seq samples from a validated gene expression pipeline (see “Materials and Methods” for details, Supplementary Fig. S1) from the Tempus database (Fig. 1). Approximately 3% of these samples ($N = 1708$) were from cancers with an unknown primary site of origin (CUPs), which were withheld from model development and used only for downstream validation and model interrogation. For the remaining samples ($N = 52,936$), we assigned one

of 68 subtype labels based on clinical documentation and a standardized abstraction protocol (see Diagnostic subtype assignment in Materials and Methods).

To evaluate the appropriateness of the cancer subtype labels for tumor origin classification, three pathologists assessed 118 randomly selected, blinded, deidentified cases, and were asked to assign a label to each case. For 109/118 cases (92%), the three pathologists agreed in their assignment. Treating those “consensus pathologist” annotations as the gold standard, the diagnostic subtype assignment method was 98% accurate (107/109). On the full 118 sample dataset, the concordance of each pathologist with the automated assignment was 92% (109/118), 94% (111/118), and 97% (114/118).

3.2 Model Performance on Labeled Samples

We applied the trained Tempus Tumor Origin (TO) model to the independent validation dataset to assess overall performance. As the Tempus TO model outputs a probability that a sample belongs to a given label, we calculated performance on the basis of the highest probability label assigned to a sample (Table 1). The model accuracy was 91.1% (95% CI 90.5–91.6%); this number approximates the probability that a random sample (with known subtype) from our laboratory is correctly predicted by the RNA-based classifier. As accuracy overemphasizes the most common cancers in our dataset, such as colorectal adenocarcinoma, we also assessed performance using mean sensitivity, which balances the impact of rare and common subtypes (see “Material and Methods”). In the validation cohort, we achieved a mean sensitivity of 80.0% (95% CI 77.9–81.7%). Sensitivity per subtype ranged from 25.9% (small bowel adenocarcinoma) to 100% in ependymoma, Ewing sarcoma, meningioma, renal chromophobe carcinoma, and schwannoma (Fig. 2). Full results of all metrics for each subtype are listed in Supplementary Table S3.

Since our classifier outputs a probability that a sample belongs to one of 68 different subtypes, we hypothesized that mislabeled samples might be correctly identified within the top N predicted subtypes. When considering the top N predicted subtypes—i.e., a prediction is deemed correct as long as the correct label is among the top N predictions[37]—we observed considerable increases in overall accuracy. Crucially, for subtypes that were most difficult to predict, the correct prediction was frequently the second highest predicted subtype, and many subtypes are predicted perfectly when considering the top three highest predictions (Fig. 3). Overall, this shows that when the model makes an incorrect prediction, the correct prediction is very often either the next highest prediction or among the top three. The top- k recall ($k = 1, 2, 3$) for all subtypes is provided in Supplementary Table S6.

To assess the possibility of performance drift over time, and to ensure model generalizability, we examined accuracy separately across a retrospective cohort (data available at the time of training but computationally withheld) and a set of samples sequenced after model freeze (Supplementary Table S7). We found no significant difference in accuracy (91.2% and 90.8%, respectively; Fisher's exact test, $p = 0.6$), further indicating that the model is generalizable. Model performance was found to be robust to tumor purities down to 10%, showing an accuracy of at least 89% for all purity bins above 10% (Supplementary Table S8). Further, there was only a small reduction in performance when applied to cases with imputed metastatic, nonmetastatic, and unknown primary status—as defined via curated sample metadata and pathological review (Supplementary Table S9).

While overall metrics of model accuracy are critical for assessing performance, these single numbers obscure the actual patterns of correct and incorrect predictions. We therefore examined confusion matrices (predicted versus observed subtype counts) for several clinically relevant groupings of subtypes (Supplementary Fig. S2). As expected, there are molecular similarities between less common gastrointestinal subtypes such as goblet cell adenocarcinoma and small bowel adenocarcinoma and more common subtypes such as colorectal adenocarcinoma. Furthermore, the confusion matrices demonstrate robust per-label sensitivity across liver and lymph node tissue sites. Full model predictions for validation set samples are included in Supplementary Table S10.

Lastly, we note that a small percent of predictions yielded ambiguous results. These samples were flagged (and not-called) whenever the largest predicted probability [the $\max(p)$ value] from among the 68 possible labels is below 35%. Among validation set samples, this occurred 1% of the

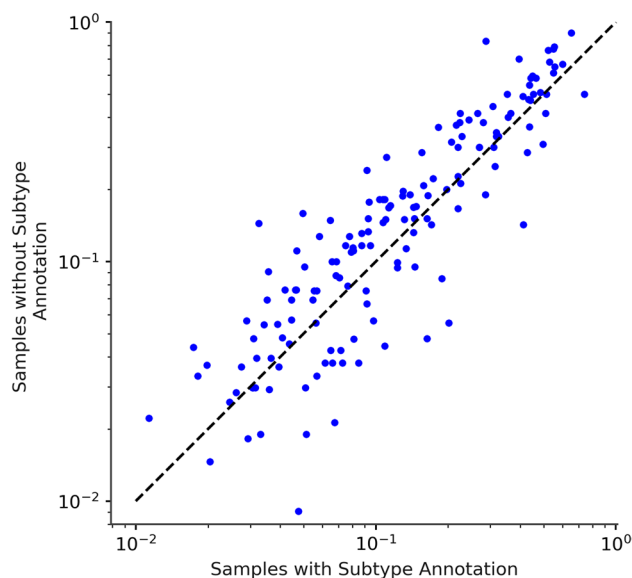


Fig. 4. Somatic mutation frequencies are compared for tumors of known origin (labels obtained from clinical data) and tumors of unknown origin (labels predicted by the Tempus TO classifier). Each point represents the somatic mutation frequency for a particular gene and subtype; all gene–subtype pairs passing the labeled-cohort significance threshold are included

time. Samples passing the $\max(p)$ threshold had a marginally higher accuracy (91.7%). However, throughout this paper, we reported all metrics according to the more pessimistic scenario where the largest predicted probability is reported regardless of whether it is below 35%. In clinical applications of the model, however, samples with $\max(p)$ below 35% will be reported as indeterminate.

Table 2 Observed somatic mutation frequency (in the labeled and CUP cohorts) of the ten most significant enrichments in the CUP cohort. See Supplementary Table S14 for the full list

Subtype	Gene	Somatic mutation frequency			
		Within subtype		Outside subtype	
		Labeled cohort	CUP cohort	Labeled cohort	CUP cohort
Pancreatic adenocarcinoma	<i>KRAS</i>	0.530	0.681	0.101	0.132
Lung adenocarcinoma	<i>STK11</i>	0.092	0.241	0.007	0.019
Cholangiocarcinoma	<i>IDH1</i>	0.079	0.109	0.011	0.002
Lung adenocarcinoma	<i>KEAP1</i>	0.050	0.159	0.003	0.014
Colorectal adenocarcinoma	<i>APC</i>	0.496	0.309	0.025	0.036
Lung adenocarcinoma	<i>SMARCA4</i>	0.032	0.144	0.007	0.026
Small cell lung carcinoma	<i>RB1</i>	0.436	0.365	0.035	0.053
Cholangiocarcinoma	<i>BAP1</i>	0.075	0.117	0.007	0.017
Skin squamous and basal cell carcinoma	<i>NOTCH1</i>	0.229	0.333	0.011	0.014
Skin squamous and basal cell carcinoma	<i>NOTCH2</i>	0.111	0.273	0.006	0.005

3.3 Generalization to TCGA Samples

To assess the generalizability of the classifier beyond samples sequenced at Tempus, we performed an analysis of TCGA samples. Despite the classifier never having seen TCGA data, the possibility of technical batch effects based on differences in sample collection and RNA-sequencing protocols, and the challenges involved in mapping ground truth subtype labels across the two datasets (see “Materials and Methods”), the overall accuracy of the TO classifier was 84.3% on TCGA samples that encompass 38 histological subtypes and the mean sensitivity was 85.2%—both values are on par with the reported accuracy from our retrospective and post-freeze validation sets. Full TCGA performance metrics are presented in Supplementary Tables S11 and S12, with full confusion matrices for Tempus and TCGA shown in Supplementary Figs. S3 and S4. To further help understand the sample-level predictions of the model, Supplementary Table S13 contains TO model predictions for all TCGA samples that passed RNA quality control. Finally, Supplementary Fig. S5 assesses the similarity in per-class sensitivity across the Tempus and TCGA datasets for all subtypes having at least three samples.

3.4 Mutation–Subtype Associations in CUP Sample Predictions

Previous analyses were performed on samples of known primary for the purpose of model training and validation, but true CUP samples may present particularly unique challenges. Assessing performance of the TO classifier on CUP samples—which, by definition, have no known subtype—is difficult but many DNA alterations are associated with specific cancer subtypes [38]. While we note that DNA variant information is not diagnostically sufficient for establishing tumor subtype, we hypothesized that mutation–subtype associations in the DNA data of labeled samples should be similar to associations found among the predicted subtypes of CUP samples (see Methods). Because the Tempus TO model is fully blind to DNA sequence variant data during training and inference, this analysis provides an independent self-consistency characterization of the classifier in the CUP setting.

For each subtype and gene alteration (SNV, indels), we selected significant mutation–subtype associations, identifying 158 enrichments in the labeled cohort (see Methods); these significant associations involved 29 subtypes and 71 genes. We next asked whether these same associations were observed in CUP samples, and were able to recover positive subtype–gene associations (i.e., subtype–gene odds ratios > 1) in 150 of the 158 cases (94.9% of associations recovered; 95% CI 91.5–98.3%) despite our model having no

explicit knowledge of sequence variants. Finally, the somatic mutation frequencies from the known subtype are recapitulated in CUP samples with the corresponding predicted subtype (Table 2, Fig. 4). Overall, this assessment found that TO predictions on CUP samples are able to recapitulate known mutation–subtype associations and is a further indicator of the consistency of the TO classifier.

4 Discussion

Improving outcomes for patients with CUP remains an unmet clinical need. Given the increasingly low cost and widespread availability of genomic testing, machine learning approaches—such as the one developed and validated here—promise to improve clinical management for patients with CUP by providing a specific anatomic and histologic diagnosis. We show that the Tempus TO assay achieves a 91% classification accuracy across 68 well-defined and clinically relevant tumor subtypes using only RNA expression data, which is quantified as part of the Tempus xT sequencing assay. These predictions are made available on a timeline comparable to the delivery of the xT test result, which is typically between 10 and 14 days after sample receipt, which is a common and clinically meaningful turnaround time for NGS test results. To further validate the Tempus TO assay and ensure its robustness, we assessed a number of orthogonal metrics for measuring classification accuracy, ensured accuracy on independent cohorts that were either held out during model development or sequenced after freezing the model, and finally showed that subtype predictions are capable of recapitulating subtype-specific mutational patterns. We additionally evaluated the TO model in TCGA data to demonstrate generalizability and found comparable performance to the internal validation sets.

An extension of the value that comes with the diagnostic resolution of CUPs provided by Tempus TO is the potential impact on therapeutic decision-making as it relates to supporting National Comprehensive Cancer Network (NCCN) recommended guidelines and Food and Drug Administration (FDA) label indications in both non-biomarker and biomarker-dependent contexts. The non-biomarker context highlights an application of Tempus TO beyond the traditional CUP setting to aid in the evaluation of tumors with a clear primary site of origin but conflicting or ambiguous histology. In lung cancer for instance, the choice to give bevacizumab in combination with carboplatin and paclitaxel is dependent on a differential diagnosis between lung adenocarcinoma and lung squamous carcinoma [39]. However, lung tumors can present with poorly differentiated histology, limiting further classification beyond “non-small cell lung cancer” [40] and complicating the ability to follow histology-specific guideline recommendations. Therefore,

a critical component of any subtype classifier is the ability to discriminate between histologies. The Tempus TO assay has sensitivity to differentiate between lung squamous cell carcinoma (sensitivity 0.88), lung adenocarcinoma (0.95), small cell lung carcinoma (0.87), and neuroendocrine lung tumors (0.43) with less tissue than is typically required for IHC (Supplementary Fig. S2). Judicious use of IHC in small tissue samples to determine a histological diagnosis is recommended to conserve tumor tissue, especially in patients with advanced disease or limited biopsy material [41, 42].

Biomarker-dependent contexts highlight the value of Tempus TO paired with targeted molecular profiling assays, such as Tempus xT, where diagnostic predictions can support biomarker and cancer type-specific therapy indications. An example of this would be differentiating diagnostically challenging upper gastrointestinal neoplasms such as gastroesophageal carcinoma, cholangiocarcinoma, hepatocellular carcinoma, pancreatic adenocarcinoma, pancreatic neuroendocrine tumors, small bowel adenocarcinoma, gastrointestinal neuroendocrine carcinomas, and well-differentiated gastrointestinal neuroendocrine tumors (Supplementary Fig. S2). With the clinical approval of *FGFR2* [43] and *IDH1* [44] targeting therapies in cholangiocarcinoma, accurate diagnosis and mutational analysis of this rare tumor subtype has the potential to support on-label therapeutic options.

Despite the high accuracy of the Tempus TO model, there are nevertheless several caveats that we wish to emphasize as possible limitations and areas for ongoing research.

First, any diagnostic algorithm for patients with CUP presents innate evaluation challenges since CUPs do not—by definition—have ground-truth labels to use in evaluation. Analytical performance can be evaluated only on cancers with an adjudicated diagnosis—calling into question the generalizability of model performance to the intended population of the assay. However, we partially addressed this challenge using DNA associations in the CUP population as an orthogonal assessment. A supporting example from the DNA analysis is the enrichment of *SMARCA4* alterations in lung adenocarcinomas (Table 2). *SMARCA4* is one of the catalytic subunits of the SWI/SNF chromosomal remodeling complex, a critical transcriptional regulator. *SMARCA4* lung cancers have been shown to be associated with poor histologic differentiation and a lack of TTF1 staining, which is a commonly used IHC biomarker for diagnosing lung cancer [45]. Although *SMARCA4* mutations are not entirely specific for lung, our analysis finds that *SMARCA4* mutations are significantly associated with lung adenocarcinoma in both CUP and non-CUP settings—but with an almost five-fold higher somatic mutation rate in the CUP cohort. Therefore, our finding of enrichment of *SMARCA4* variants in patients with CUP

predicted as lung adenocarcinoma is an expected finding given the diagnostic challenge posed by TTF1 negative, poorly differentiated carcinomas [46].

Second, performance metrics such as overall accuracy are dependent on the case distribution observed in our laboratory, which may differ from other institutions as well as the general population. To mitigate the effect of differing case distributions, we additionally report per-label sensitivity and specificity for use in evaluating each label in isolation (Supplementary Table S3). It should be noted that one of the expected drivers of misclassification in the TO test is the overlapping nature of gene expression profiles for cancers with similar histologies such as squamous cell carcinomas from several primary sites, or cancers of differing histology but from the same site. Evaluation of confusion matrices that illustrate per-label performance identify similar trends of misclassification attributable to this expected limitation in both the Tempus and TCGA data (Supplementary Figs. S3 and S4). Additionally regarding possible TCGA to Tempus per-label discordance, there were expected limitations in the mapping of TCGA and Tempus labels and different diagnostic practice variability such as with the evolving World Health Organization (WHO) classification of gliomas [47].

Third, while our label set is comprehensive, it does not represent all possible cancer subtypes. In clinical practice, a CUP case may be presented to the classifier where the true diagnosis is not well represented in the 68 diagnostic cancer subtypes or is unlike any case observed in the training set. Examples of such cases may include rare de novo histologic variants of common cancers such as sarcomatoid variants. The resulting predictions in these settings can still inform the possible site of origin and the histologic subtype; however, oversight by the ordering physician is required to integrate molecular predictions with all available clinical evidence to aid in subtype diagnosis.

Fourth, this study focused specifically on RNA expression-based prediction, but additional data modalities (e.g., digital pathology, fusions, DNA) might allow for expansion of the diagnostic label and reportable range of the assay. This is particularly relevant in the context of cancer subtypes with pathognomonic alterations such as *BRD4-NUT* fusions in NUT midline carcinoma.

Fifth, some cancer subtypes can transition from one histological diagnosis to another. For example, prostate and lung adenocarcinomas can acquire neuroendocrine histology in response to treatment with ADT [48] and EGFR inhibitors [49], respectively. It can be challenging to assign a precise diagnosis in situations where a tumor has a mixed or transitioning histology. Tempus TO identifies the prominent histological subtype in a tumor specimen, enabling better clinical management.

Finally, this study focused on assessing diagnostic accuracy using samples with known labels. We demonstrated high accuracy on a set of samples that were collected and analyzed after freezing the development of our model and therefore illustrate the ability of our model to generalize. Future studies that may be valuable include truly prospective tests of diagnostic accuracy such as those that rely on clinical follow-up or even postmortem primary identification following the determination of a predicted subtype. Future studies of clinical utility will also be valuable, such as studies investigating changes in medication utilization or survival endpoints.

5 Conclusion

The present study has demonstrated the high accuracy and granularity of a cancer subtype predictor (Tempus TO) for use in classifying cancers of unknown or uncertain primary origin. The subtype predictor was built using one of the largest known collections of paired RNA-seq and subtype labels and distinguishes between 68 subtypes with an overall accuracy of 91%. We anticipate that Tempus TO will be a useful tool for providing physicians with a precise histological and site-specific diagnosis, an essential component for clinical decision-making in the increasingly detailed landscape of precision medicine.

Supplementary Information The online version contains supplementary material available at <https://doi.org/10.1007/s40291-023-00650-5>.

Acknowledgements The authors acknowledge that a version of this manuscript was posted as a preprint on medRxiv (<https://doi.org/10.1101/2022.05.06.22274683>).

Declarations

Funding Funding for this project and open access was provided directly by Tempus Labs.

Conflicts of interest All authors are employees, former employees, and/or hold restricted stock units of Tempus Labs, Inc.

Availability of data and material Raw data for this study were generated at Tempus Labs. Derived data supporting the findings of this study are available within the paper and its Supplementary Figs./Tables. Requests for additional data should be addressed to publication.inquiry@tempus.com. Due to the clinical nature of these samples, requests will be evaluated by a Data Access Review Group and are subject to a signed data transfer agreement.

Ethics approval Analyses were performed using de-identified data under the exemption Pro00042950, granted from the Advarra, Inc Institutional Review Board (IRB) on 15 April 2020 based on the Department of Health and Human Services regulations found at “45 CFR 46.104(d)(4).” All methods were carried out in accordance with relevant guidelines and regulations. Internal validations and laboratory

protocols were developed and performed in a CLIA-certified, CAP-accredited laboratory.

Consent to participate Written informed consent is not required from the subject/s or legal guardians per the above-stated exemption (consent was exempted by Advarra Inc. Institutional Review Board).

Consent for publication N/A.

Code availability N/A.

Author contributions JM, AB, JK, AJH, JG, KAB, and TT conceptualized the work. BM performed wet-lab experiments. JM, KM, NB, MS, RJ, EM, KAB, and TT curated data. MB, AB, JK, KM, CM, and KAB wrote the software. JM and JK provided the formal analysis and validation. MCS, NB, MS, RJ, EM, KB, JG, KAB, and TT supervised the work. JM, KM, AJH, JG, KAB, and TT contributed to data visualization. All authors participated in drafting the manuscript. JM, JK, KM, AJH, CI, JTD, MCS, NB, JG, KAB, and TT edited the manuscript.

Open Access This article is licensed under a Creative Commons Attribution-NonCommercial 4.0 International License, which permits any non-commercial use, sharing, adaptation, distribution and reproduction in any medium or format, as long as you give appropriate credit to the original author(s) and the source, provide a link to the Creative Commons licence, and indicate if changes were made. The images or other third party material in this article are included in the article's Creative Commons licence, unless indicated otherwise in a credit line to the material. If material is not included in the article's Creative Commons licence and your intended use is not permitted by statutory regulation or exceeds the permitted use, you will need to obtain permission directly from the copyright holder. To view a copy of this licence, visit <http://creativecommons.org/licenses/by-nc/4.0/>.


References

- Benson AB, Venook AP, Al-Hawary MM, Arain MA, Chen Y-J, Ciombor KK, et al. Colon cancer, version 2.2021, NCCN clinical practice guidelines in oncology. *J Natl Compr Canc Netw*. 2021;19:329–59.
- Varadhachary GR, Raber MN. Cancer of unknown primary site. *N Engl J Med*. 2014;371:757–65.
- Fizazi K, Greco FA, Pavlidis N, Daugaard G, Oien K, Pentheroudakis G, et al. Cancers of unknown primary site: ESMO clinical practice guidelines for diagnosis, treatment and follow-up. *Ann Oncol*. 2015;26(Suppl 5):v133–8.
- National Comprehensive Cancer Network. Occult Primary, Version 2.2021, NCCN Clinical Practice Guidelines in Oncology. *J Natl Compr Canc Netw*.
- Key statistics for cancers of unknown primary [Internet]. [cited 2021 Apr 13]. Available from: <https://www.cancer.org/cancer/cancer-unknown-primary/about/key-statistics.html>
- Mnatsakanyan E, Tung W-C, Caine B, Smith-Gagen J. Cancer of unknown primary: time trends in incidence. *United States Cancer Causes Control*. 2014;25:747–57.
- Massard C, Lorient Y, Fizazi K. Carcinomas of an unknown primary origin—diagnosis and treatment. *Nat Rev Clin Oncol*. 2011;8:701–10.
- Hayashi H, Takiguchi Y, Minami H, Akiyoshi K, Segawa Y, Ueda H, et al. Site-specific and targeted therapy based on molecular profiling by next-generation sequencing for cancer of unknown primary site: a nonrandomized phase 2 clinical trial. *JAMA Oncol*. 2020;6:1931–8.

9. Golub TR, Slonim DK, Tamayo P, Huard C, Gaasenbeek M, Mesirov JP, et al. Molecular classification of cancer: class discovery and class prediction by gene expression monitoring. *Science*. 1999;286:531–7.
10. Ramaswamy S, Tamayo P, Rifkin R, Mukherjee S, Yeang CH, Angelo M, et al. Multiclass cancer diagnosis using tumor gene expression signatures. *Proc Natl Acad Sci U S A*. 2001;98:15149–54.
11. Rassy E, Pavlidis N. Progress in refining the clinical management of cancer of unknown primary in the molecular era. *Nat Rev Clin Oncol*. 2020;17:541–54.
12. Varadhachary GR, Spector Y, Abbruzzese JL, Rosenwald S, Wang H, Aharonov R, et al. Prospective gene signature study using microRNA to identify the tissue of origin in patients with carcinoma of unknown primary. *Clin Cancer Res*. 2011;17:4063–70.
13. Ferracin M, Pedriali M, Veronese A, Zagatti B, Gafà R, Magri E, et al. MicroRNA profiling for the identification of cancers with unknown primary tissue-of-origin. *J Pathol*. 2011;225:43–53.
14. Pillai R, Deeter R, Rigl CT, Nystrom JS, Miller MH, Buturovic L, et al. Validation and reproducibility of a microarray-based gene expression test for tumor identification in formalin-fixed, paraffin-embedded specimens. *J Mol Diagn*. 2011;13:48–56.
15. Grewal JK, Tessier-Cloutier B, Jones M, Gakkhar S, Ma Y, Moore R, et al. Application of a neural network whole transcriptome-based pan-cancer method for diagnosis of primary and metastatic cancers. *JAMA Netw Open*. 2019;2: e192597.
16. Zhao Y, Pan Z, Namburi S, Pattison A, Posner A, Balachander S, et al. CUP-AI-Dx: A tool for inferring cancer tissue of origin and molecular subtype using RNA gene-expression data and artificial intelligence. *EBioMedicine*. 2020;61: 103030.
17. Penson A, Camacho N, Zheng Y, Varghese AM, Al-Ahmadie H, Razavi P, et al. Development of genome-derived tumor type prediction to inform clinical cancer care. *JAMA Oncol*. 2019. <https://doi.org/10.1001/jamaoncol.2019.3985>.
18. Jiao W, Atwal G, Polak P, Karlic R, Cuppen E, et al. A deep learning system accurately classifies primary and metastatic cancers using passenger mutation patterns. *Nat Commun*. 2020;11:728.
19. Liu MC, Oxnard GR, Klein EA, Swanton C, Seiden MV. CCGA Consortium Sensitive and specific multi-cancer detection and localization using methylation signatures in cell-free DNA. *Ann Oncol*. 2020;31:745–59.
20. Lu MY, Chen TY, Williamson DFK, Zhao M, Shady M, Lipkova J, et al. AI-based pathology predicts origins for cancers of unknown primary. *Nature*. 2021;594:106–10.
21. Ma X-J, Patel R, Wang X, Salunga R, Murage J, Desai R, et al. Molecular classification of human cancers using a 92-gene real-time quantitative polymerase chain reaction assay. *Arch Pathol Lab Med*. 2006;130:465–73.
22. Erlander MG, Ma X-J, Kesty NC, Bao L, Salunga R, Schnabel CA. Performance and clinical evaluation of the 92-gene real-time PCR assay for tumor classification. *J Mol Diagn*. 2011;13:493–503.
23. Kerr SE, Schnabel CA, Sullivan PS, Zhang Y, Singh V, Carey B, et al. Multisite validation study to determine performance characteristics of a 92-gene molecular cancer classifier. *Clin Cancer Res*. 2012;18:3952–60.
24. Hainsworth JD, Rubin MS, Spigel DR, Boccia RV, Raby S, Quinn R, et al. Molecular gene expression profiling to predict the tissue of origin and direct site-specific therapy in patients with carcinoma of unknown primary site: a prospective trial of the Sarah Cannon research institute. *J Clin Oncol*. 2013;31:217–23.
25. Abraham J, Heimberger AB, Marshall J, Heath E, Drabick J, Helmstetter A, et al. Machine learning analysis using 77,044 genomic and transcriptomic profiles to accurately predict tumor type. *Transl Oncol*. 2021;14: 101016.
26. Handorf CR, Kulkarni A, Grenert JP, Weiss LM, Rogers WM, Kim OS, et al. A multicenter study directly comparing the diagnostic accuracy of gene expression profiling and immunohistochemistry for primary site identification in metastatic tumors. *Am J Surg Pathol*. 2013;37:1067–75.
27. Vibert J, Pierron G, Benoist C, Gruel N, Guillemot D, Vincent-Salomon A, et al. Identification of tissue of origin and guided therapeutic applications in cancers of unknown primary using deep learning and RNA sequencing (TransCUPtomics). *J Mol Diagn*. 2021;23:1380–92.
28. Beaubier N, Tell R, Lau D, Parsons JR, Bush S, Perera J, et al. Clinical validation of the Tempus xT next-generation targeted oncology sequencing assay. *Oncotarget*. 2019;10:2384–96.
29. Beaubier N, Bontrager M, Huether R, Igartua C, Lau D, Tell R, et al. Integrated genomic profiling expands clinical options for patients with cancer. *Nat Biotechnol*. 2019;37:1351–60.
30. Cieslik M, Chugh R, Wu Y-M, Wu M, Brennan C, Lonigro R, et al. The use of exome capture RNA-seq for highly degraded RNA with application to clinical cancer sequencing. *Genome Res*. 2015;25:1372–81.
31. xGen Exome Research Panel [Internet]. Integrated DNA Technologies; 2020. Available from: <https://www.idtdna.com/pages/products/next-generation-sequencing/targeted-sequencing/hybridization-capture/pre-designed-panels/xgen-exome-research-panel-v2>
32. Anders S, Huber W. Differential expression analysis for sequence count data. *Genome Biol*. 2010;11:R106.
33. Hu J, Parsons J, Mineo B, Bell JSK, Malinauskas J, Drews J, et al. Abstract 2239: Comprehensive validation of RNA sequencing for clinical NGS fusion genes and RNA expression reporting. *Cancer Res*. American Association for Cancer Research; 2021;81:2239–2239.
34. SEQC/MAQC-III Consortium. A comprehensive assessment of RNA-seq accuracy, reproducibility and information content by the Sequencing Quality Control Consortium. *Nat Biotechnol*. 2014;32:903–14.
35. The Cancer Genome Atlas program [Internet]. National Cancer Institute. 2018 [cited 2022 Mar 18]. Available from: <https://www.cancer.gov/tcga>
36. Network CGA. Comprehensive molecular characterization of human colon and rectal cancer. *Nature*. 2012;487:330–7.
37. Lu MY, Chen TY, Williamson DFK, Zhao M, Shady M, Lipkova J, et al. AI-based pathology predicts origins for cancers of unknown primary. *Nature*. 2021. <https://doi.org/10.1038/s41586-021-03512-4>.
38. Haigis KM, Cichowski K, Elledge SJ. Tissue-specificity in cancer: the rule, not the exception. *Science*. 2019;363:1150–1.
39. NCCN Guidelines Non-Small Cell Lung Cancer [Internet]. National Comprehensive Cancer Network; 2020 Dec. Available from: https://www.nccn.org/professionals/physician_gls/pdf/nscl.pdf
40. Paech DC, Weston AR, Pavlakis N, Gill A, Rajan N, Barraclough H, et al. A systematic review of the interobserver variability for histology in the differentiation between squamous and nonsquamous non-small cell lung cancer. *J Thorac Oncol*. 2011;6:55–63.
41. Moreira AL, Thornton RH. Personalized medicine for non-small-cell lung cancer: implications of recent advances in tissue acquisition for molecular and histologic testing. *Clin Lung Cancer*. 2012;13:334–9.
42. Yatabe Y, Dacic S, Borczuk AC, Warth A, Russell PA, Lantuejoul S, et al. Best practices recommendations for diagnostic immunohistochemistry in lung cancer. *J Thorac Oncol*. 2019;14:377–407.
43. Center for Drug Evaluation, Research. FDA grants accelerated approval to pemigatinib for cholangiocarcinoma [Internet]. 2020 [cited 2021 Sep 3]. Available from: <https://www.fda.gov/drugs/resources-information-approved-drugs/fda-grants-accelerated-approval-pemigatinib-cholangiocarcinoma-fgfr2-rearrangement-or-fusion>

44. Center for Drug Evaluation, Research. FDA approves ivosidenib for advanced or metastatic cholangiocarcinoma [Internet]. 2021 [cited 2021 Sep 3]. Available from: <https://www.fda.gov/drugs/resources-information-approved-drugs/fda-approves-ivosidenib-advanced-or-metastatic-cholangiocarcinoma>
45. Agaimy A, Fuchs F, Moskalev EA, Sirbu H, Hartmann A, Haller F. SMARCA4-deficient pulmonary adenocarcinoma: clinicopathological, immunohistochemical, and molecular characteristics of a novel aggressive neoplasm with a consistent TTF1neg/CK7pos/HepPar-1pos immunophenotype. *Virchows Arch.* 2017;471:599–609.
46. Nambirajan A, Singh V, Bhardwaj N, Mittal S, Kumar S, Jain D. SMARCA4/BRG1-deficient non-small cell lung carcinomas: a case series and review of the literature. *Arch Pathol Lab Med.* 2021;145:90–8.
47. Louis DN, Perry A, Wesseling P, Brat DJ, Cree IA, Figarella-Branger D, et al. The 2021 WHO classification of tumors of the central nervous system: a summary. *Neuro Oncol.* 2021;23:1231–51.
48. Patel GK, Chugh N, Tripathi M. Neuroendocrine differentiation of prostate cancer-an intriguing example of tumor evolution at play. *Cancers.* 2019. <https://doi.org/10.3390/cancers11101405>.
49. Marcoux N, Gettinger SN, O’Kane G, Arbour KC, Neal JW, Husain H, et al. EGFR-mutant adenocarcinomas that transform to small-cell lung cancer and other neuroendocrine carcinomas: clinical outcomes. *J Clin Oncol.* 2019;37:278–85.

Authors and Affiliations

Jackson Michuda¹ · Alessandra Breschi¹ · Joshua Kapilivsky¹ · Kabir Manghnani¹ · Calvin McCarter¹ · Adam J. Hockenberry¹ · Brittany Mineo¹ · Catherine Igartua¹ · Joel T. Dudley¹ · Martin C. Stumpe¹ · Nike Beaubier¹ · Maryam Shirazi¹ · Ryan Jones¹ · Elizabeth Morency¹ · Kim Blackwell¹ · Justin Guinney¹ · Kyle A. Beauchamp¹  · Timothy Taxter¹

Jackson Michuda
jack.michuda@tempus.com

Alessandra Breschi
alessandra.breschi@tempus.com

Joshua Kapilivsky
joshuah.kapilivsky@tempus.com

Kabir Manghnani
kabir.manghnani@tempus.com

Calvin McCarter
calvin.mccarter@tempus.com

Adam J. Hockenberry
adam.hockenberry@tempus.com

Brittany Mineo
brittany.mineo@tempus.com

Catherine Igartua
katie.igartua@tempus.com

Joel T. Dudley
joel.dudley@tempus.com

Martin C. Stumpe
martin.stumpe@tempus.com

Nike Beaubier
nike.beaubier@tempus.com

Maryam Shirazi
maryam.shirazi@tempus.com

Ryan Jones
ryan.jones@tempus.com

Elizabeth Morency
elizabeth.morency@tempus.com

Kim Blackwell
kim.blackwell@tempus.com

Justin Guinney
justin.guinney@tempus.com

¹ Tempus Labs, Chicago, IL 60654, USA